UCRL-52616

NONDESTRUCTIVE, ENERGY-DISPERSIVE X-RAY FLUORESCENCE ANALYSIS OF PRODUCT-STREAM CONCENTRATIONS FROM REPROCESSED LWR FUELS

D. C. Camp

W. D. Ruhter

S. Benjamin

January 5, 1979

Work performed under the auspices of the U.S. Department of Energy by the UCLLL under contract number W-7405-ENG-48

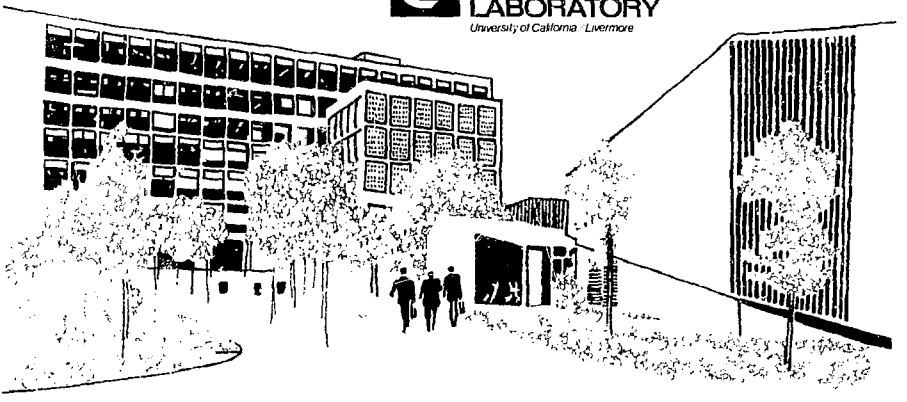

Distribution Category
UC-78

LAWRENCE LIVERMORE LABORATORY
University of California Livermore, California 94550

UCRL-52616

NONDESTRUCTIVE, ENERGY-DISPERSIVE X-RAY FLUORESCENCE ANALYSIS OF PRODUCT-STREAM CONCENTRATIONS FROM REPROCESSED LWR FUELS

D.C. Camp

W. D. Ruhter

S. Benjamin*

MS. date: January 5, 1979

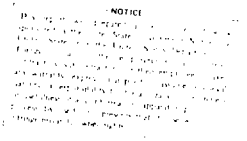

*Student visitor, LLL 1978 summer program.

PREFACE

This report presents results of research and development (R&D) funded by the Department of Energy (DOE) and administered by the Savannah River Laboratory (SRL). The DOE-sponsored program dealt, in general, with the Alternative Fuel Cycle Technology Program. Lawrence Livermore Laboratory's role was to assess the adaptability of selected x- and gamma-ray techniques. The instruments and techniques considered were applicable to the nondestructive analysis of the output products from reprocessed light water reactor fuel. The R&D program, begun in Fiscal 1978, was to have continued for at least three years; however, a sudden redirection of the DOE program announced during the last two days of FY 78, terminated the work. Therefore, the results presented in this report are only partial and the discussion must be understood in the context of an unfinished R&D program.

CONTENTS

Preface ii
Abstract 1
Introduction 1
Product Accountability 1
Overview of XRFA 2
Experimental Equipment 3
Excitation Source Requirements 3
Solution Cells 5
Computer-Based Analyzer 5
Experimental Procedures and Results 6
Spectra 6
Count Rate vs Concentration and Cell Calibration 10
Dynamic Concentration Measurements 13
Concentration Changes vs Acid Normality 14
Future Research and Development Needs 18
Mechanical Requirements 18
Electronic Requirements 18
Computer Software Requirements 19
Solution Requirements 19
References 21
Appendix 22
Concentration Measurement Procedures and Equations 22

NONDESTRUCTIVE, ENERGY-DISPERSIVE X-RAY FLUORESCENCE ANALYSIS OF PRODUCT-STREAM CONCENTRATIONS FROM REPROCESSED LWR FUELS

ABSTRACT

Energy-dispersive x-ray fluorescence analysis can be used for quantitative on-line monitoring of the product concentrations in single- or dual-element process streams in a reprocessing plant. The 122-keV gamma ray from ^{57}Co is used to excite the K x-rays of uranium and/or plutonium in nitric acid solution streams. A collimated HPGe detector is used to measure the excited x-ray intensities. Net solution radioactivity may be measured by eclipsing the exciting radiation, or by measuring it simultaneously with a second detector. The technique is nondestructive and noninvasive, and is easily adapted directly to pipes containing the solution of interest.

The dynamic range of the technique extends from below 1 to 500 g/l. Measurement times depend on concentration, but better than 1% counting statistics can be obtained in 100 s for 400 g/l concentrations, and in 1000 s for as little as 10 g/l. Calibration accuracies of 0.3% or better over the entire dynamic range can be achieved easily using carefully prepared standards. Computer-based analysis equipment allows concentration changes in flowing streams to be dynamically monitored. Changes in acid normality of the stream will affect the concentration determined, hence it must also be determined by measuring the intensity of a transmitted ^{57}Co beam. The computer/disk-based pulse-height analysis system allows all necessary calculations to be done on-line. Experimental requirements for an in-plant installation or a test and evaluation are discussed.

INTRODUCTION

Product Accountability

In the event that nuclear fuel from light water reactors (LWR) is reprocessed to reclaim the uranium and/or plutonium, several analytical techniques will be used for product accountability. Generally, the isotopic content of both the plutonium and uranium in the reprocessed product will have to be accurately determined. One plan for the reprocessing of LWR spent fuel incorporates the following scheme.[1] After separation from both the fission products and transplutonium actinides (including neptunium and americium), part of the uranium and all of the plutonium in nitrate solution will merge to form a coprocessed stream. This solution will be concentrated by evaporation and sent to a holding tank for accountability. Input concentrations into the holding tank are expected to be approximately 350 g of uranium per liter and nearly 50 g of plutonium per liter. The variation to be expected in these concentrations is not known. The remaining uranium fraction will be further purified and sent to a separate storage tank. Its expected stream concentration will be about 60 g of uranium per liter. These two relatively high stream concentrations can be monitored rapidly, quantitatively, and nondestructively using the technique of energy-dispersive x-ray fluorescence analysis (XRFA).

Eventually, the mixed product stream will be coprecipitated and converted to a powder blend of uranium and plutonium oxide. This product is referred to as mixed oxide or simply MOX, and will be packaged in 2000 g amounts. Since incoming LWR fuel bundles from different reactors will not have the same burnup, the elemental and isotopic composition of the various MOX batches will vary. This means that for accountability, inventory control, and subsequently fuel fabrication purposes, there will be a need to know

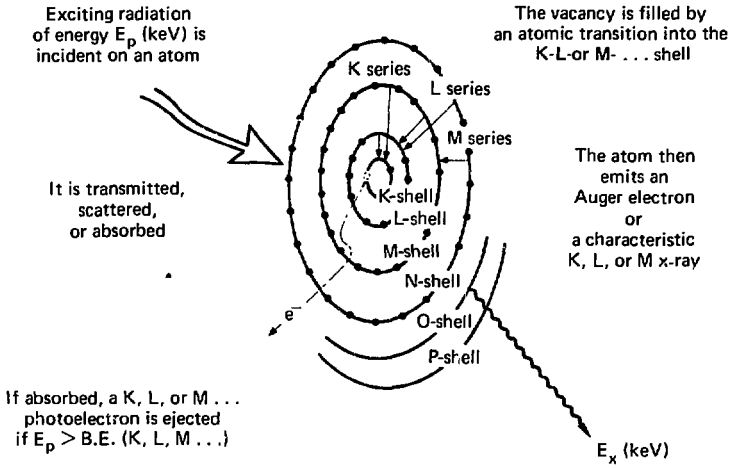

Fig. 1. A simplified schematic representation of energy-dispersive x-ray fluorescence analysis. The number of electrons within a given shell and the number of major shells depend on the particular atom. (B.E. stands for binding energy.)

the percentage of enrichment of plutonium in each MOX container and batch. Futhermore, since fissionability of the product when refabricated will also be important, the isotopic composition of the product will need to be determined. Gamma-ray spectroscopy of the product canisters can be used to nondestructively assay both the enrichment and isotopics of the MOX. A detailed description of this measurement procedure can be found in another report.[2]

Overview of XRFA

The analytical technique of XRFA depends upon the ability to excite atoms within a sample and to measure accurately the characteristic x rays emitted from the excited atoms. The atoms may be excited in many different ways. These include the use of ordinary x-ray tubes, with or without filtered anodes; irradiation by α, β, γ, or x rays from radioisotopes; bombardment by charged particles from accelerators; bombardment by electrons, as in electron microprobes; irradiation by secondary x rays from a selected target element, or by polarized x or γ rays such as from synchrotron radiation; self-excitation, if the sample contains radioactivity; and by observing x rays that follow certain nuclear decay modes.

Phenomenologically, XRFA can be understood as follows. Assume that a flux of exciting radiation composed of photons of energy, E_p, is incident on a sample. A small part of the incident radiation flux may not interact with the sample at all; another part may scatter, either with or without some energy loss; or part of the flux may be completely absorbed by the sample. Although there may be millions of such interactions throughout the sample, each interaction takes place with a single atom. A simplified representation of one interaction is illustrated in Fig. 1. If the incident quantum is totally absorbed, and if E_p (keV) is greater than the binding energy of some electron in the atom, then one of the atom's electrons will be ejected. This creates a vacancy in one of the atomic shells, which leaves the atom in an excited or unstable condition.

If the vacancy created is in the K-shell, then it may be filled by an electron that falls from a less tightly bound shell into the inner shell vacancy. This results in either the emission of one of the atom's characteristic x rays or an Auger electron (which rarely escapes the sample). If an x ray is emitted and escapes the sample, it is available for spectroscopic analysis. Since all of the characteristic x rays associated with an element are well-known, it is possible to identify most of the elemental constituents of a sample through x ray fluorescence analysis.

The use of this analytical technique has spread quickly into many different professional disciplines. The principal reasons are found in the technique's advantages:

- It has wide dynamic range, i.e., concentration measurements from ppb to %.
- Quantitative analysis can be rapid, i.e., from 0.10 s to 10.0 min.
- It is nondestructive to the sample.
- Sample preparation time is usually minimal to none.
- The sample form can be as a solid, liquid, or gas.
- Multielement analysis is possible, even down to sodium ($Z = 11$).
- The spectral interpretation is almost unambiguous.
- Data output is digital, hence computerizable.
- Routine analyses are easily automated, so the cost goes down.
- Automated systems are simple to operate by trained technicians.

A more detailed discussion of the fundamental principles of energy dispersive x-ray fluorescence analysis can be found in Ref. 3.

Because of these advantages, energy-dispersive x-ray fluorescence analysis can be used to measure LWR reprocessed product-stream concentrations nondestructively, noninvasively, and with sufficient accuracy. The following section will describe the required experimental apparatus and computer-based analytical support instrumentation. The Experimental Procedure and Results section will present data obtained on single- and dual-element nitrate solutions with typical concentrations expected at an LWR reprocessing facility. The last section in the report will discuss the research and development still needed before this technique can be considered ready for in-plant installation and application, or before an in-plant test and evaluation can be carried out.

EXPERIMENTAL EQUIPMENT

Excitation Source Requirements

Gamma rays can be used to excite x rays from atoms within a sample. The binding energies of K electrons in uranium and plutonium are 115.59 and 121.72 keV, respectively. Since the primary gamma ray emitted by ^{57}Co has an energy of 122.05 keV, it is an optimum exciting radiation for these two elements. Depending on the geometry of the sample, the exciting radiation is usually collimated in some fashion. This is to reduce the amount of radiation that can scatter off nonsample materials or that can fluoresce them.

Lithium-drifted silicon, Si(Li), is an excellent radiation detector for x rays with less than 30 keV of energy, but it becomes very inefficient for the detection of radiation energies above 60 keV. Since the K x-ray energies of uranium and plutonium extend from 98 to 120 keV, a lithium-drifted or high-purity germanium detector, Ge(Li) or HPGe, is used. For this work a 10-mm-deep, 200-mm^2 HPGe detector was used. It had an energy resolution of 600 eV FWHM for the 122.05-keV gamma-ray peak of ^{57}Co.

The source-detector collimation assembly is shown in Fig. 2. Two ^{57}Co sources are partially collimated to create two beams. The radioactivity was electroplated onto a 1.6-mm-diam spot and encased in a welded stainless steel capsule 4.8 mm in diameter by 3.2-mm thick. These capsules* are supported by counterbored aluminum cylinders machined such that they point upwards at a small angle. The axes of the two loosely collimated beams make an angle of approximately 30° with respect to the detector collimation axis. The 0.37-mm-thick stainless steel plate indicated in Fig. 2 is part of the bottom of a glove box, which was used when handling all of the solutions. The source-detector collimation assembly and liquid nitrogen (LN) dewar are separate from and located below the glove box. The collimator assembly is 7.5 cm in diameter and 5.0-cm thick.

Since ^{57}Co also emits 570- and 692-keV gamma rays with branching intensities of about 0.16%, as well as other weaker gamma rays above 300 keV, their intensities must be strongly attenuated by introducing shielding between the source and the detector. X rays from lead and heavimet (tungsten alloy) can also be excited by the source gamma rays; hence, graded absorbers of cadmium and copper are used as liners on the top and bottom surfaces to eliminate these x rays. A central 12.5-mm hole within this collimator assembly allows part of the x rays fluoresced within the sample to strike the detector.

In the application of interest here the sample is a solution contained within a cylindrical geometry. A solution cell or pipe section used for calibration purposes could have any diameter, but should be larger than the inside diameter of the detector's collimator. The collimated 122-keV gamma rays interact with atoms in the solution, creating x rays characteristic of those elements dissolved in the solution. A portion of the emitted x rays are collimated to strike the detector,

*Available from Isotopes Products Laboratories, Burbank, CA.

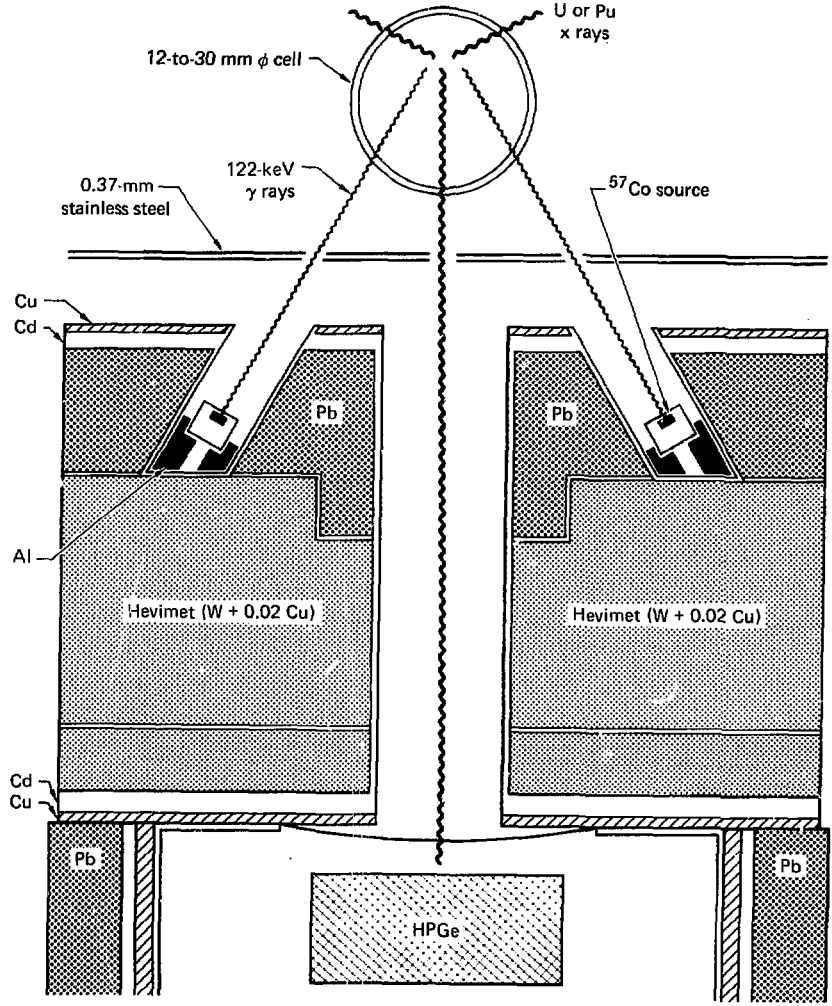

Fig. 2. *A cross-sectional view of the circular source exciter and detector collimator assembly.* The 0.37-mm stainless steel plate is part of the bottom of a glove-box assembly. The cell can represent a pipe or calibration solution cell.

and from the energies and intensities detected, the elemental concentrations in the solution can be determined.

The HPGe detector cryostat used in these experiments utilized a beryllium window, but such a window is not necessary if the actinide K x-rays are to be detected. Clearly, the x-ray intensity recorded by the HPGe detector increases as the sample volume-to-detector distance decreases. However, this distance cannot be decreased indefinitely. As the distance is decreased, less shielding is possible between the intense ^{57}Co sources and the detector. Those higher energy gamma rays, which pass through the heavimet and interact with the HPGe detector, create a Compton continuum that appears as a constant, energy-independent background in the vicinity of the uranium and plutonium x rays. This noise contribution increases very rapidly with decreasing amounts of shielding, degrading the x ray signal-to-noise ratio quickly. Some high Z shielding is also required around the detector housing (above the cryostat) to reduce background radiation detected from the local environment and source-air scattering.

The radiation sources and detector collimator are necessarily coupled to the detector and its LN dewar, which was located below the glove box containing the solution cell. A glove box must be used when handling solutions containing plutonium, so that in the event of a spill, contamination is confined. The LN dewar was supported by a platform bolted to the frame supporting the glove box. This positive coupling of the dewar to the glove box was necessary because spatial alignment must be maintained between the solution cells within the glove box and the detector collimation axis outside the box. The dewar was mechanically decoupled from the glove box frame by 12 mm of foam rubber between the glove box and platform and the platform and dewar. This prevented mechanically induced microphonics from the glove box, its frame, or the floor from coupling into the detector.

Solution Cells

In an actual reprocessing plant, uranium and plutonium nitrate solutions will probably flow through stainless steel pipes. To examine the behavior of concentrated uranium and plutonium nitrate solution under flowing conditions, a flow system was constructed. A photograph of this system is shown in Fig. 3. A variable speed, peristaltic pump moves the solution through the tygon tubing and cell by a cyclical squeezing action. The solution circulates from the separatory funnel through the cell and pump, and then is returned to the funnel. The flow direction can be reversed if desired.

Calibrated, unknown, or wash nitric acid solutions containing only uranium were transferred from their containers to the separatory funnel by the unidirectional air flow hand pump. This avoided any pouring action. Quantitative transfers were usually not necessary. By reversing the dual-channel stopcock, the flow system could be emptied using the peristaltic pump. Since 2 to 3% of the solution remains in the tubing, the system was flushed out after each use, and then primed with a solution close in concentration to the next to be measured. The glass cell allowed visual inspection of the flow conditions. Three sizes of pyrex cells, 12, 25, and 38 mm in outside diameter, were used.

Once it was demonstrated that the fluoresced x-ray intensities were independent of whether the solution was flowing or static, solution cells were constructed using stainless steel. Each cell was machined to have an outside diameter of 18.80 mm and 3.00-mm thick walls. They had a nominal solution length of 10.0 cm. Bottoms were heliarced to the tubes, whereas the tops of the tubes were threaded internally. The tops for these tubes contained a recessed O-ring and a partially threaded, axially centered, 6/32 fill hole. The stainless steel cells were filled nearly completely, then the top was inserted with silicone sealant applied to the threads and a silicon based O-ring was used. The remaining volume of the tube was filled through the small 6/32 fill hole to eliminate any air bubbles. Then, a 6/32 machine screw with silicone sealer on its threads was inserted. After 24 hr each cell was decontaminated and inspected for leaks. Stainless steel cells filled with plutonium nitrate or mixed uranium-plutonium nitrate must be handled in a sealed glove box environment. To ensure repeatability in the measurements, both the pyrex cells and stainless steel cells could be positively located in a reproducible position with respect to the detector collimation axis.

Computer-Based Analyzer

The x rays fluoresced in the solution samples are detected by the HPGe detector. Preamplified pulses are routed to a Canberra 1413 amplifier and 1468A pile-up rejector. Valid output pulses are routed to a Nuclear Data ND600 pulse height analyzer (PHA). The PHA with its own LSI-11 microprocessor is coupled to an LSI-11 minicomputer that has a 32k, 16-bit word memory. A dual floppy disk unit is coupled to the LSI-11 and each disk has a 216k byte (108k word) capacity. Other system peripherals include a Hazeltine video teletypewriter terminal, an LA-180 high-speed line printer, and a Tektronix digital data plotter.

A computer-based pulse height analyzer adds a considerable amount of versatility to the experimental

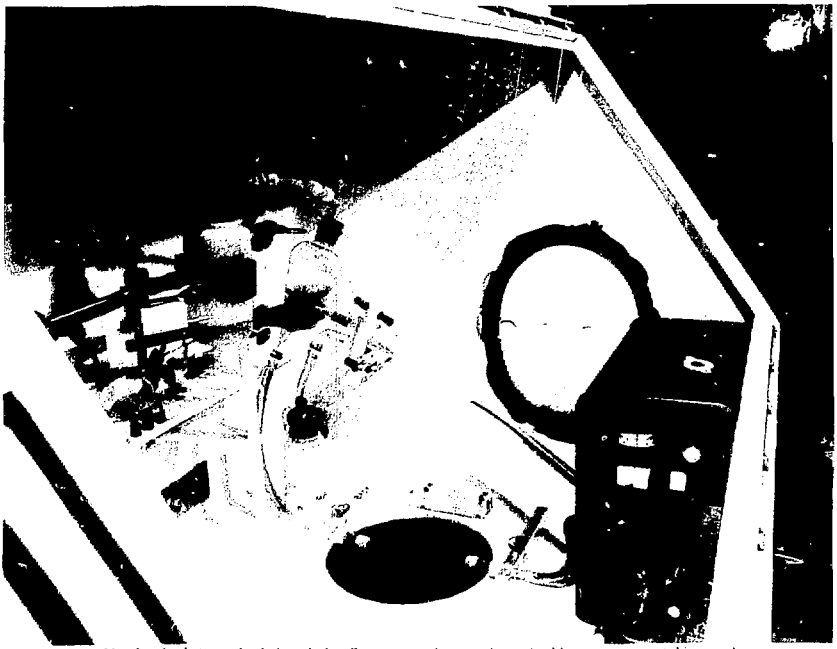

Fig. 3. A photograph of the solution flow system showing the peristaltic pump, tygon tubing, and 25-mm diam pyrex cell. Note that the cell is locked in position. The dual channel stopcock allows drainage of the system.

system. In fact, in an actual reprocessing installation a computer based data analysis system would be essential, and would probably be linked to a command computer center. This particular system allowed successive spectra to be stored on disk, and permitted spectrum analysis to be carried out simultaneously while data were also being acquired. With [illegible] sequence is desired, appropriate [illegible] ten and stored on floppy [illegible] programs can be written in FORTRAN [illegible] another language for use in the [illegible]

EXPERIMENTAL PROCEDURES AND RESULTS

Spectra

The spectrum shown in Fig. 4 is the result of an x-ray fluorescence analysis of pure uranium nitrate solution at 100 g U/l contained in a 25-mm diam, cylindrical pyrex cell. Total analysis time was 334 live time seconds at 19.4% analyzer dead time using two 5 mCi ^{57}Co sources. The net Kα1 x ray intensity is almost 2 x 10^5 counts. The energy region shown extends from 90 to 200 keV. One of the more dominant features in the spectrum is the broad, intense peak centered at about channel 450. This peak is a result of the primary exciting radiation (the 122 keV gamma ray of ^{57}Co) incoherently or Compton scattering through an angle of 140

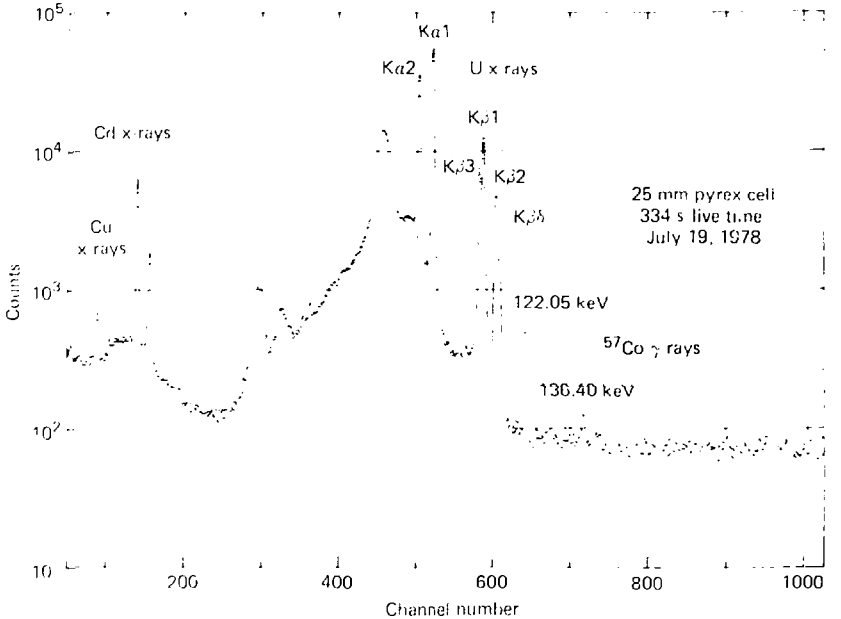

Fig. 4. A 1024-channel x-ray fluorescence analysis spectrum of 100 g U/L uranium nitrate in the 25-mm cell. The cadmium x rays result from a liner of the inner wall of the detector collimator. The two broad peaks above channel 500 are incoherently scattered platinum (source backing material) x rays.

The sharp, intense peaks located between channel 500 and 620 are the K x rays of uranium. The most intense x ray is $K\alpha 1$ of uranium at 98.439 keV. The $K\alpha 2$ is about half as intense and located slightly lower in energy at 94.665 keV. The $K\beta$ x rays contain more than one component, hence appear as multiplets. The ($K\beta 1' + K\beta 3 + K\beta 5$) x ray is located near channel 584, while ($K\beta 2' + K\beta 4' + K\delta$) is less intense and located about channel 608. The weak 122 keV peak at about channel 644 is coherently scattered (no energy change) exciting radiation. The very weak peak observed at channel 720 is the coherently scattered 136.4-keV gamma ray also from ^{57}Co. Its intensity is one-tenth that of the 122 keV radiation. The short, nearly flat distribution centered about channel 488 is the 140 incoherently scattered radiation from the 136.4 keV gamma ray.

The other features in the spectrum are of minor importance. The two sharp peaks located at about channel 150 are the $K\alpha$ and $K\beta$ x rays from cadmium, which lined the central wall of the beam/net collimator. The two broad peaks near channel 300 are incoherently scattered x rays of platinum. The ^{57}Co radioactivity was electroplated on platinum disks. The flat continuum extending above channel 650 is the low energy portion of the Compton distribution arising primarily from the 570- and 692 keV gamma rays emitted by ^{57}Co.

Figure 5 shows an expanded view of a fluorescence spectrum of the 80-to 130-keV region for two different concentrations of uranium in nitric acid. The most intense spectrum represents a concentration of 350 g U/L, whereas the weaker spectrum results from a nitrate solution containing only 3.5 g U/L. These two spectra span a dynamic concentration range of 100. The actual dynamic range offered by the XRFA technique is in excess of 1000; however, it is most useful for concentrations above 1 g U/L. Below 1 g U/L the counting times required become much longer in order to obtain sufficient statistical accuracy.

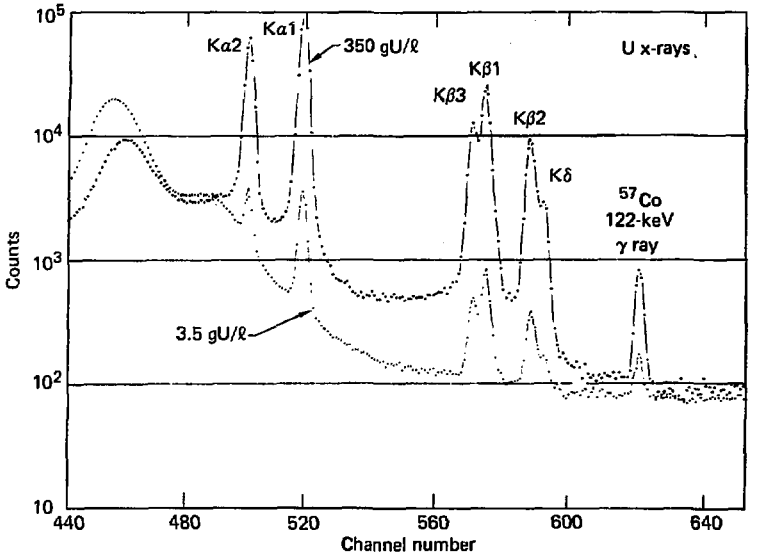

Fig. 5. Two spectra of uranium x rays in the 80-to-130-keV region for two concentrations of uranium nitrate plotted for equivalent counting times. Note the behavior of the incoherent and coherent scattering peaks of the 122-keV exciting radiation vs concentration.

Note that as the solution concentration increases, the intensity of the coherently scattered exciting radiation peak at 122 keV increases (because the effective Z of the solution increases). Also, as the solution concentration increases, the broad incoherent or Compton-scattered 122-keV peak at about 85 keV decreases in intensity and shifts slightly toward a higher energy. The increase in energy of this peak from 3.5 to 350 g U/l is 0.79 keV, which corresponds to a change from 143.6° to 138.7° in the backscattering angle. In effect, at higher concentrations the center of the solution volume fluoresced moves slightly closer to the detector, thus decreasing the backscattering angle.

The top spectrum in Fig. 6 shows an expanded view of the 80-to-130-keV region of uranium and plutonium nitrate solution. The uranium concentration is 350 g U/l, whereas the plutonium concentration is 48 g Pu/l. This mixture corresponds closely to the uranium-plutonium concentration ratio expected to flow into the final holding tank from a nonspiked, coprocessed product stream. The principal features in this spectrum are the fluoresced x rays of uranium and plutonium, and several plutonium gamma rays from its natural radioactivity. The natural radioactivity arising from this uranium-plutonium solution is shown in the lower spectrum, which has been plotted one decade lower for clarity. All features in the spectrum have been identified; however, many of these are quite different than those expected in the XRFA of a freshly reprocessed uranium-plutonium nitrate stream. These differences merit some discussion.

The major difference is that weapons-grade plutonium was used to make up the mixed solution. Also, uranium slightly depleted in ^{235}U relative to its natural abundance was used. Table 1 lists the approximate isotopic percentages for uranium and plutonium used in making the mixed solution, and compares these data with the isotopics expected in freshly reprocessed spent fuel.

Table 1. Approximate uranium and plutonium isotopics in %.

Uranium isotope	Fig. 6	35,000 MWd/t spent fuel		Fig. 6	Plutonium isotope
			2.0	< 0.01	238
235	0.5	0.8	6.0	93.5	239
236	—	0.5	22	5.9	240
238	99.5	98.7	12	0.6	241
			4	—	242
			—	≈ 0.2	(^{241}Am)

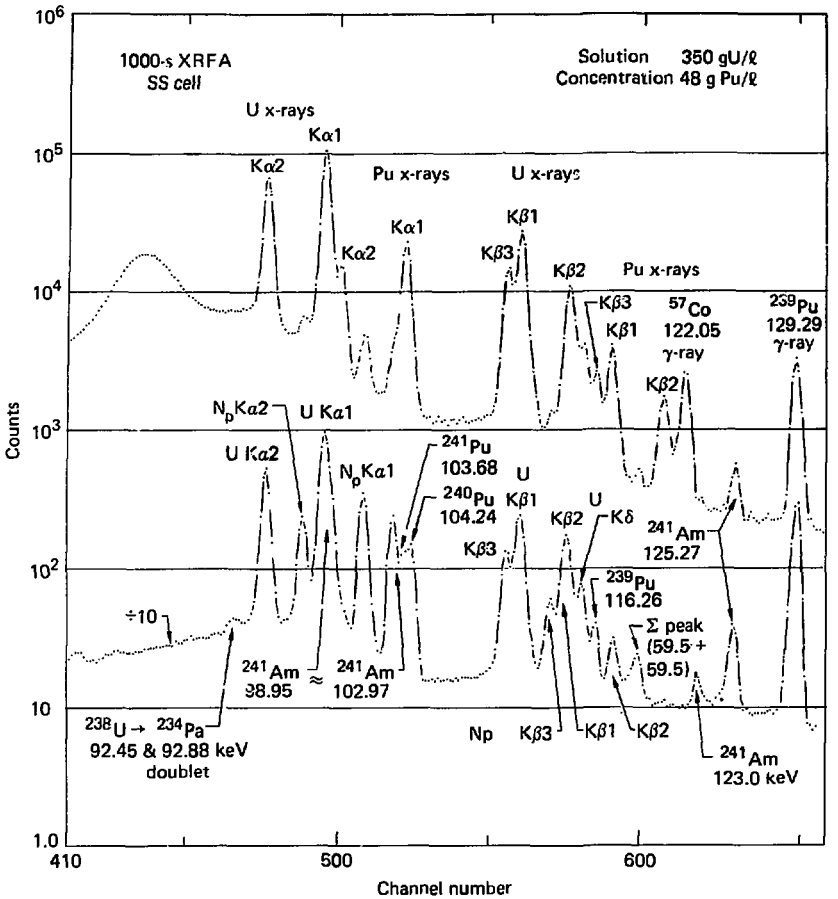

Fig. 6. The top spectrum is an XRFA of a mixed uranium-plutonium nitrate solution in a stainless steel cell. Their respective concentrations are shown. The lower spectrum results from the natural radioactivity in the solution. It is plotted one decade lower for clarity, that is, the 129.29 keV peak from ^{239}Pu in the top spectrum results entirely from the solution's natural radioactivity.

The different isotopics will have the following consequences on the natural radioactivity issuing from a freshly reprocessed uranium-plutonium nitrate stream:

- The 92.45- and 92.88-keV doublet gamma ray in ^{234}U from the decay of ^{238}U will still be present, but will not be significantly troublesome.
- The neptunium K x-ray intensity that accompanies the decay of ^{237}U and ^{241}Am should be less intense.
- The ^{241}Am, which has been chemically separated, will not have its 98.95-, 102.97-, 123.0-, and 125.29-keV gamma rays present.

- Also, the (59.53 + 59.53-keV) sum peak at 119.06 keV will be absent.
- The ^{241}Pu, 103.68-keV gamma ray will be much stronger.
- The ^{240}Pu, 104.24-keV gamma ray will also be stronger.
- The ^{239}Pu gamma-ray lines at 98.71-, 116.26-, 124.5-, and 129.29-keV will not be as strong.

Finally, it is difficult to say how strong the uranium K x-ray lines will be from natural radioactivity. They will grow in strength as the α decay of ^{241}Pu approaches equilibrium, about 42 d. A small contribution from internal α and γ self-fluorescence may be present but will depend on solution concentration. Any separated ^{237}U blended back into the coprocessed stream will contribute to the neptunium K x-ray intensity. Since the plutonium isotopics will not remain the same from fuel batch to batch, the natural radioactivity in the coprocessed stream will have to monitored. Thus, it appears that in the x-ray fluoresced spectrum, uranium Kα1 and plutonium Kα2 will be relatively free of interference, but plutonium Kα1 will have strong contributions from the ^{240}Pu, 104.24-keV and the ^{241}Pu, 103.68-keV gamma rays. So far, there are no plans to determine or use the Kβ x-ray intensities from either isotope.

Count Rate vs Concentration and Cell Calibration

A set of standard solutions was prepared using ACS-grade natural uranium nitrate. Sufficient HNO_3 acid was used to adjust the acid concentration to 3.0 *M*. The standards covered the range 0.6 to 350 g U/l and their values were determined by potential coulometry. The solutions were introduced into the flow system as described earlier. The 25-mm-diam pyrex cell was the first to be used and Fig. 4 showed a spectrum obtained from the *100 g U/l solution. Generally, to obtain data* for each concentration, three separate runs were made with the system under flow (or static) conditions once or twice out of the three runs. Analysis live times for each run were set to obtain better than 0.5% statistics (40,000 counts) in the gross Kα1 peak, but no run was less than 100 s. Only one long run was used to obtain data on solution concentrations $\leq$1 g U/l. Subsequently, this procedure was repeated for the 12-mm-diam pyrex cell. For the 38-mm-diam pyrex cell and stainless steel cell, data were obtained with the solution not flowing (static). Other extensive experiments had confirmed that concentration measurements made on the solution under flow or static conditions were equivalent (see next section).

Figure 7 shows the net counting rate in counts per second (left border) in the uranium Kα1 peak as a function of solution concentration (top border) as measured with the 25-mm-diam pyrex cell. The two similarly shaped curves below this give the count rate observed in the plutonium Kα1 or uranium Kα1 for unmixed solutions of plutonium or uranium nitrate, respectively, in the stainless steel cell. The small figures in parentheses indicate the analyzer dead times in percent for 100 g/l solution concentrations in each cell type. The plutonium solution contained natural radioactivity, whereas the uranium solution in the stainless steel cell contained less solution volume than the 25-mm-diam pyrex cell, hence its lower dead time.

As the solution concentration is increased, there is less than a linear increase in the count rate. This fall off in count rate is a combination of increasing self-absorption of the Kα1 x ray within the solution and an effective decrease in the solution volume fluoresced as the concentration is increased. Clearly, the net count rate observed will depend on the ^{57}Co source strength ($T_{1/2}$ = 270 d), the experimental geometry and cell wall thickness, and the HPGe detector efficiency. Such a simple count rate vs concentration curve is not time independent. Furthermore, at high concentrations the rate of change of count rate with concentration becomes less sensitive (i.e., a 1% change in count rate corresponds to a 4% change in concentration at 300 g U/l for the 25-mm cell). The observed count rate is also sensitive to minor changes in geometry and system dead time, which varies with concentration. Air bubbles in a flowing stream would also affect the observed count rate. So, it is desirable to define a calibration procedure that is independent of source half-life and system dead time, insensitive to minor changes in geometry and stream flow conditions, and more sensitive to concentration changes.

It can be seen from the two spectra in Fig. 5 that as the fluoresced x-ray intensity increases, the 140° incoherently scattered, 122-keV radiation at 86 keV decreases. *The ratio of the Kα1 x-ray intensity to a* portion of the spectrum that includes the incoherent peak is almost independent of concentration. If this ratio is plotted vs concentration on log-log paper, the slope is observed to *increase* slightly for concentrations in excess of 30 g U/l. The concentration in g/l can be related to this ratio through the relationship

$$C = K \left[\frac{GK\alpha 1}{GI} - B \right], \qquad (1)$$

where GKα1 is the gross counts within a window including the Kα1 x-ray peak, GI is the gross counts in a window including the incoherent peak, and K is a calibration constant in g/l. The constant B is the ratio GKα1/GI for pure nitric acid. This ratio is independent

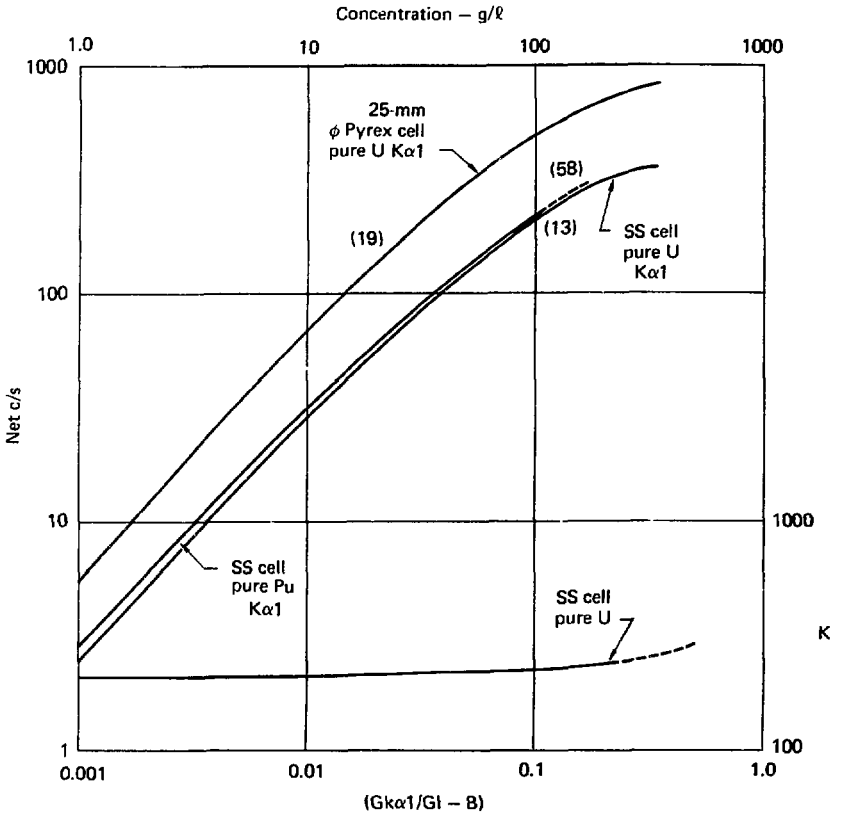

Fig. 7. A log-log plot of the measured net count rate (left) vs solution concentration (top) for single-element solutions in the pyrex and stainless steel cell. The lower curve shows the behavior of the calibration constant K (right) vs the experimental determined ratio (bottom).

of source exciter half-life, changes in dead time, and small changes in geometry. Thus, the bracketed quantity in Eq. (1) is an experimentally measurable quantity. If a well-defined relationship of K vs the bracketed quantity can be established, then their product will yield the concentration.

The lower portion of Fig. 7 shows the behavior of K (right border) vs this ratio (lower border) for the stainless steel cell containing pure uranium nitrate solution. The increase in K at higher concentrations is effectively a result of increasing self-absorption of the uranium Kα1 and decreasing fluoresced volume as the solution concentration increases. A least-squares fit to K, expressed as a polynomial function of the natural logarithm of the bracketed quantity, results in the equation shown as an inset at the top of Fig. 8. This figure shows the percentage deviation between the calculated and experimental K as a function of solution concentration in the stainless steel cell. The mean absolute value difference is 0.34% with a root-mean-square deviation of 0.20%. A similar equation was defined for each of the three pyrex cells, and Table 2 lists

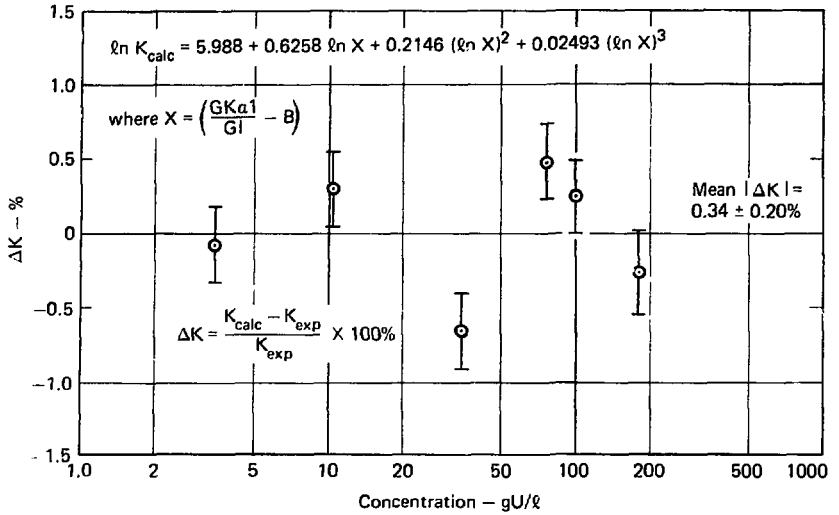

Fig. 8. A semilog plot for the residuals ΔK vs the concentration. The equation used to calculate K is shown. The mean | ΔK | is 0.34 ± 0.20%.

results for ΔK. The solution concentrations were initially determined by potential coulometry and subsequently were measured by the same technique two months later. The errors in the concentration represent half the maximum total change in concentration observed. The solution having a concentration of 78 g U/l was initially made up as an unknown with a concentration of 78.6 g U/l. The value obtained for this solution for the 25-mm-diam cell, and using the appropriate equation for K, yielded a value of 78.3 ± 0.3 g U/l, 0.6% above the mean solution value of 77.84. Since the 25-mm cell was the first to be used, the experimen-

TABLE 2. Percent difference between calculated and experimental K vs concentration.

Uranium nitrate in 3.0 *M* HNO_3		Pyrex cell, o.d. in mm			Stainless steel cell, o.d., in mm
g U/l	% error	12	25	38	18
3.524 ± 0.026	0.74	−0.04	0.00	−0.08	−0.07
10.14 ± 0.14	1.38	0.16	−0.02	0.30	0.30
34.91 ± 0.07	0.20	−0.31	0.03	−0.57	−0.66
77.84 ± 0.80	1.03	—	(+0.59 ± 0.38)	−0.13	0.47
99.79 ± 0.15	0.15	0.35	−0.04	0.87	0.24
179.45 ± 0.45	0.25	−0.16	0.02	−0.39	−0.27
350 − 332[a]	—				—
|Mean| %	0.63	0.20	0.022	0.039	0.034
	±0.50	±0.12	±0.015	±0.29	±0.20

[a]The 350 g U/l solution was made up in 3.6 *M* HNO_3 and also showed the largest change over a 2-mo period. Although data were taken with each cell using this standard, it cannot be used in defining an equation for K because of its different molarity.

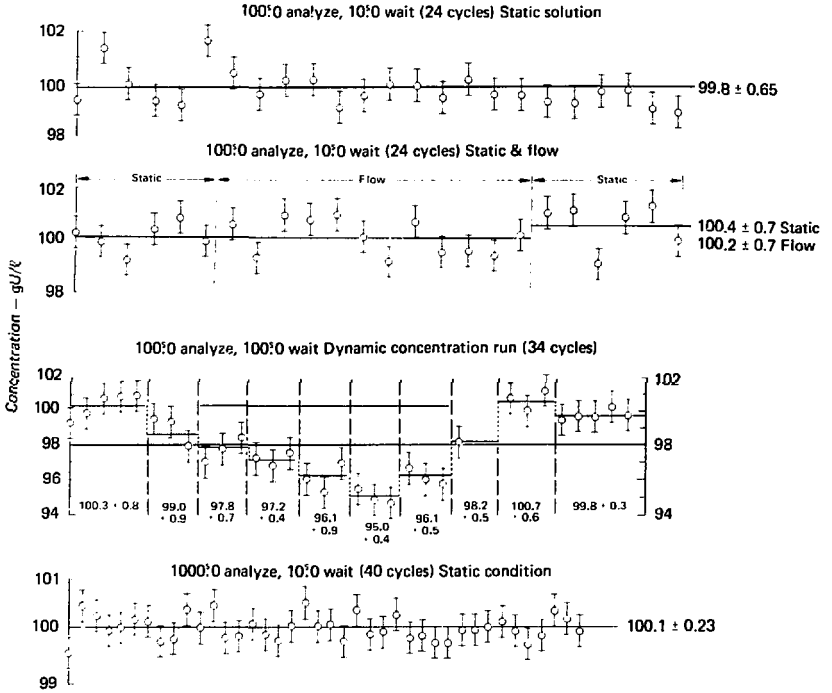

Fig. 9. Four plots of solution concentration vs time. The analysis time and pause times vary. The top set of data points was taken with the solution static; the second with the first and last six measurements static, the center 12 flowing; the third is a dynamic concentration run (see text); and the last again static. The error bars indicate statistical counting accuracy only.

tally measured value indicates very probably the actual concentration of the unknown solution at that time of measurement. A much smaller concentration range would be expected at an actual monitoring station, hence numerous solution standards could be made that would surround the expected value and lead to an even more accurate calibration than obtained here.

Dynamic Concentration Measurements

One of the advantages of the pyrex cell (coupled to the peristaltic pump via tygon tubing) is the ability to observe the solution under flow or static conditions while a measurement is in progress. In order to verify that the two conditions yield equivalent results, the following experiment was conducted. The ND-600 disk-based, analyzer system was programmed to carry out an analysis for a preset time, Δt , in seconds, store the results on disk, clear the memory, and begin a new analysis, again for Δt s. Data transfer and memory clearance required a minimum of 10 s. This cycle could be repeated n times, where n was a preselected integer. Data could be taken in this manner with the solution either static or flowing.

Concentration results obtained with the 25-mm-diam pyrex cell using the 100 g U/l solution in static mode are shown in the topmost section of Fig. 9. Here n was set to 24 and Δt was set to 100 s. This analysis time gave on an average about 57,000 counts gross in the uranium Kα1 peak region and 89,500 counts in the incoherent window. This defined an overall statistical

standard deviation for each measurement of 0.53%. Repeating this measurement 24 times could not improve this precision. Only by making a longer measurement could the statistical standard deviation, hence the precision of the concentration, have been improved. The resulting mean standard deviation for the 24 measurements of 0.65%, which was larger than 0.53%, suggested an unknown and unaccounted for variable present in the measurement.

The second section of Fig. 9 shows a similar set of 24 measurements; however, the first and last six measurements were made with the solution static, whereas the central 12 measurements were made with the solution flowing at 80 l/hr (approximately the flow rate of the product output stream in the conceptual reprocessing plant). The static and flow results overlap well within the precision of the standard error of both means, which are slightly larger (0.70%) than the 24-cycle static run (0.65%).

Another advantage of the flow system is the ability to demonstrate dynamic concentration measurements. By introducing a known volume into a dry cell/tubing system, small volumes of pure 3.0 *M* HNO_3 acid can be introduced into the separatory funnel. These volumes are such as to lower the concentration by known small increments. Similarly, by introducing known volumes of a more concentrated solution, the concentration can be increased. In this manner concentration changes in an actual flowing stream can be simulated. The third section of Fig. 9 illustrates such measurements. Initially, 100.0 ml of the 100.0 g U/l standard solution was introduced into the flow system with the cell and tubing dry. Appropriate volumes of pure 3 *M* HNO_3 were calculated and measured so that they could be introduced into the flow system, resulting in a concentration reduction of exactly 1.0 g U/l for each of five times. Then, appropriate volumes of more concentrated uranium nitrate solutions were introduced to increase the entire solution volume 2.0 g U/l for each of three steps. This should bring the system to 101 g U/l, whereupon a final calculated volumetric addition of pure 3 *M* HNO_3 would return the solution to its original 100.0 g U/l concentration.

The pause time of 100 s was selected on the basis of results from earlier dynamic concentration runs. This time is somewhat longer than that required for the solution to reach equilibrium after introduction of an additional volume. Results of the dynamic concentration run are shown by the third set of results in Fig. 9. Again, each 100-s analysis had approximately the same statistical accuracy of 0.53%; however, the mean values indicated for each successive concentration change are determined from just the three (or six) measurements made. These varied from 0.9 to 0.3%. Unfortunately, for the seventh concentration change (98.2 g U/l), the data storage disk filled up and two cycles were lost. After the next concentration adjustment, data storage was continued on a new disk. Note that the mean of the first and last five dynamic concentrations yield a mean value of 100.05 ± 0.63 g U/l in excellent agreement with the mean value of 100.13 ± 0.40 from the first 48 static and static/flow cycles.

Finally, the analysis time was changed to 1000 s, n set at 40, and solution concentration measurements carried out automatically in the static mode. This improved the statistical precision on an individual measurement to 0.17%. The mean concentration determined from the 40 measurements is 100.1 g U/l (again in excellent agreement with the earlier runs), with a standard deviation of 0.23%. These data are shown in the lowest section of Fig. 9. During the first three runs, careful observation of the uranium Kα1 x-ray line revealed that the gain drifted sporadically by up to ± 0.3 channel. Subsequent experiments showed that such gain variations do introduce an additional error (fraction of 1%) in the gross area of the Kα1 peak. Recall that a fixed channel window integration method was used to obtain the gross counts. In an actual plant situation, a higher analyzer conversion gain would be used (i.e., spread a 0-to-210-keV spectrum over 4000 channels) and zero and gain stablizers would be employed. These gain drifts probably account for the increased standard deviation observed for the first two 24-cycle runs (0.65 and 0.70% vs 0.53% expected) but were not as significant during a longer 1000-s analysis time (0.23 vs 0.17% expected).

Concentration Changes vs Acid Normality

In the conceptual reprocessing plant, the solution entering the final evaporation tank will have product concentrations of 28.5 g U/l and 3.87 g Pu/l in 0.30 mol/l HNO_3. In an earlier feed adjustment step 12 mol/l HNO_3 is introduced to bring the solution molarity from 0.31 to 4.0 *M*. Depending on the accuracy of this final feed adjustment and on the final accuracy of the evaporation step, both the concentration and acid normality can be expected to vary. Therefore, it is important to investigate what effect, if any, the solution's HNO_3 molarity/l will have on concentration measurements made using the energy dispersive x-ray fluorescence analysis technique.

The essential components being measured in the concentration measurement are the intensity of the U kα1 x ray and the intensity of the Compton-scattered 122-keV radiation in the vicinity of 86 keV. If either of these quantities are altered by changes in the solution molarity, then the concentration determined will be compromised. The density of nitric acid at 20°C varies

from 1.032 g/l at 1 mol/l to 1.30 at 10 mol/l. An increase in solution density will lead to an increase in the amount of Compton scattering and the amount of solution self-absorption. The latter will decrease the observed uranium Kα1 x-ray intensity. Thus, if the solution concentration remains constant but the acid molarity increases, the ratio (GKα1/GI) must decrease; hence lead to an apparent decrease in the solution concentration for the same value of K [see Eq. (1.)]. Figure 10 shows the result of the concentration determined according to Eq. *(1)* and the K for 100 g U/l as a function of acid molarity for four solutions made up at 100.0 g U/l. The slope in the vicinity of 4.0 mol/l is about ± 1.4 g U/l per unit of molarity change. What this slope may be for other concentrations must be determined. The significance of these data for any real process line is that if a concentration change is indicated by Eq. *(1)*, it may not be real but merely a change in the solution molarity. Therefore, two measurements are needed, one to determine the concentration and a second to determine acid molarity, thereby verifying or modifying the initial concentration measurement.

At any solution concentration, an increase in HNO_3 molarity will result in an increase in the solution density. The amount of transmitted radiation through a solution decreases with increasing solution density. Hence, by measuring the intensity of a selected transmitted beam, density information can be obtained. Since the exciting radiation is loosely collimated, one could in principle use the transmitted intensity of the exciting radiation as a density monitor. Unfortunately, this would require the use of a second detector located in a rather precarious position above the cell. Furthermore, neither of the two exciting sources is sufficiently well collimated to form an ideal "beam." However, by using a third, highly collimated, ^{57}Co source positioned directly above the cell with its collimation axis colinear with the detector axis, it is possible to evaluate the solution density, hence acid molarity, at any concentration.

Consider the physics of the radiation interaction. Below 1 MeV, there are only two primary modes of radiation interaction with matter. First, there is photoelectric absorption. When it occurs, a K x-ray may be emitted. Second, there is radiation scattering. Compton or incoherent scattering degrades the original photon energy for all scattering angles, $\Theta \geq 0°$, whereas coherent scattering leaves the incident photon energy unchanged regardless of the scattering angle Θ. Thus, a beam of intensity I_0 incident on a solution cell will have four major components as shown in Eq. (2):

$$\sigma_{pe} + \sigma_{is} + \sigma_{cs} + I_t = I_0. \qquad (2)$$

The first term, photoelectric absorption, is governed by the effective atomic number of the solution in the cell

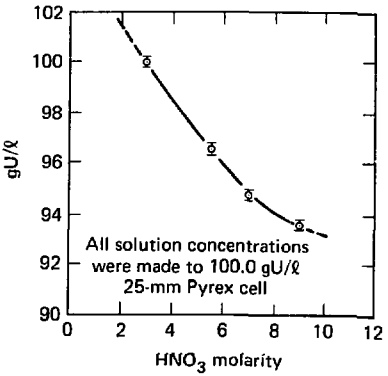

Fig. 10. A plot of the variation in the measured solution concentration with acid molarity. All solutions were made up to 100 g U/l, but their concentrations were calculated using Eq. (1) and assumed the calibration constant K for a 3 *M* solution was valid for the other molarities.

(Z_{eff}). The second term, the incoherent or Compton-scattering cross section, is governed by Z_{eff} and the solution density, ρ_{sol}. The third term, the coherent-scattering cross section, σ_{cs}, is small and depends only on Z_{eff}. The last term, the transmitted intensity, I_t, depends on Z_{eff} and ρ_{sol}. For any given cell filled with the same solution concentration, only the second and fourth terms will vary appreciably with changes in acid molarity (solution density). Any photon not transmitted must be scattered, that is, ($\sigma_{is} + I_t$) is a constant independent of solution for a given concentration. (Technically, σ_{pe} also depends on density but only the heavy element component of the total effective photoelectric cross section is measured by the uranium or plutonium Kα1 x rays, hence σ_{pe} is essentially independent of ρ_{sol}.) Any scattering angle can be chosen as a representative measure of the Compton-scattering cross section, hence that part of the gross incoherent peak area already integrated can be used. Since, the exciting source strength is much greater than the "beam" strength, that fraction of the gross incoherent area chosen to sum with the "beam" intensity will depend on the transmission source strength. So a measurement of the transmitted intensity plus an appropriate fraction of the incoherent or Compton-scattered intensity will allow a determination of acid molarity.

A series of x-ray fluorescence spectra were obtained covering four different concentrations from 3.5 to 100 g U/l prepared at each of five different acid molarities that spanned the range 1.0 to 9.0 *M*/l. A third

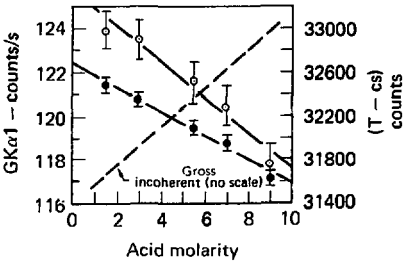

Fig. 11. Variation in the gross uranium Kα1 counts/s (solid circles); the total transmitted 122-keV intensity (T) minus the coherent scattering contribution (cs) as open circles; and an indicat of the rate of change of the gross incoherent area (dashed line). All three are plotted as a function of acid molarity for 35 g U/l solution in the stainless steel cell.

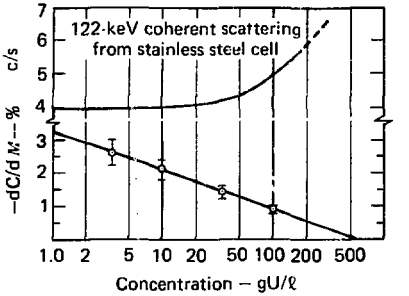

Fig. 12. The top curve shows a semilog plot of the behavior of the coherently scattered 122-keV radiation as a function of concentration for the stainless steel cell. Note the large contribution from the stainless steel cell. The lower curve shows the behavior in the negative rate of change of concentration with molarity as a function of concentration. A linear fit was assumed.

^{57}Co source was mounted above the cell position and its 1.2-mm beam aligned colinearly with the HPGe detector axis. All measurements were made with the same refillable stainless steel cell with a fiducial line marked along its side. The cell was placed in two lucite "feet" secured to the stainless steel plate in the bottom of the glove box. The lucite feet ensured that the cell was repositioned exactly from run to run, whereas the fiducial line guaranteed that the cell was placed with the same "side" up. Any variation in the thickness of the cell's wall vs length or axial position could introduce varying amounts of absorption. As will be seen, small changes in transmitted intensity are important.

Figure 11 shows results for the five 35-g U/l solution standards. As the acid molarity increases from 1.0 to 9.0 *M*, the solution density increases and the observed uranium GKα1 counts/s decreases by nearly 4%. At the same time the gross incoherent scattered peak area increases by 5% (no scale given for dashed line). Note that as was observed in Fig. 10, if each of these solution concentrations had been calculated using an equation similar to Eq. (1) and the 3.0 *M* value for K, a decrease in concentration would be observed as molarity increases (similar to Fig. 10, only steeper). Also, Fig. 11 shows that the net counts observed in the transmitted beam's 122-keV intensity decrease with increasing acid molarity. Again, increasing solution density leads to a 4% decrease in the transmitted 122-keV radiation. The total coherent-scattered (cs) contribution of 4150 counts has been subtracted. About 4000 of these counts come from the stainless steel cell walls. The increase in the 122-keV coherent-scattering count rate vs concentration is shown as the top curve in Fig. 12. For this size stainless steel cell only a small fraction of the total number of coherent-scattered events comes from pure nitric acid or uranium nitrate. The method proposed, then, is to obtain an average value for (T-cs) plus an appropriate fraction of GI for all acid molarities at each concentration. This average value should be a constant independent of acid molarity at each concentration. It will be called Σ.

Table 3 summarizes the transmission results obtained for the various acid molarities and concentrations measured. The smallest percent error in the parameter, Σ, for the source strength used here is obtained by taking 5% of the gross incoherent area, and summing it with the net transmitted 122-keV intensity to yield the parameter Σ. This 5% fraction yields the lowest average percent error for all concentrations (0.63 ± 0.17%). Note that the statistical accuracy alone is about ± 0.5% or worse for just the (T-cs) component. The fractional percentage errors in Σ at each of the individual concentrations listed in Table 3 are to be compared to the large percentage changes in calculated concentration values of 22% at 3.5 U/l to 6% at 100 g U/l, which would have occured if they had all been assumed to be 3 *M* and if their concentrations were determined by the ratio method, i.e. Eq. (1). The lower curve in Fig. 12 shows the rate of change of solution concentration per unit molarity change as obtained from concentrations calculated according to the ratio method, assuming it is applicable. This curve indicates that at low concentrations, changes in acid molarity, hence solution density, strongly affect the uranium Kα1 x-ray intensity and the incoherent-scattering contributions, thus strongly affecting the concentration results obtained. For more concentrated uranium solutions an increase in acid molarity leads to a decrease in the calculated concentration, but by smaller percentages.

Table 3. A summary of the acid molarity vs concentration results.

M	(5% GI)	+	(T-cs)	=	Constant	$\Sigma \pm \sigma$	σ, in %[a]	Concentration gU/l
9	30,350		17,734		48,084			
7	29,960		18,753		48,713			
5.5	29,925		18,364		48,289	48,290 ± 300	±0.62%	100.0
3.0	29,340		18,742		48,082			
9	33,820		31,768		65,588			
7	33,420		32,300		65,720			
5.5	33,375		32,526		65,901	65,620 ± 270	±0.41	35.0
3	32,825		32,900		65,725			
1.5	32,190		32,990		65,180			
9	35,645		36,230		71,875			
7	35,115		36,260		71,375			
5.5	34,910		38,100		73,010	72,140 ± 600	±0.83	10.3
3.0	34,115		38,170		72,285			
1.1	33,760		38,390		72,150			
9	36,145		37,130		73,275			
7	35,650		38,040		73,690			
5.5	35,210		39,050		74,260	73,560 ± 480	±0.65	3.56
3	34,590		39,010		73,600			
1.0	33,940		39,050		72,990			

[a]Average % error 0.63 ± 0.17

The actual percentage change in dC/dM probably does not go to 0, but would asymptotically approach the concentration axis. The fitted line shown intersects the axis because a linear relationship was assumed.

Figure 13 illustrates the behavior of the parameter Σ as a function of concentration. As the concentration decreases, Σ asymptotically approaches a constant. This is reasonable since both terms in the sum will approach constant values as the solution concentration approaches that of pure acid. The middle curve illustrates the behavior of the transmitted 122-keV radiation for 3 M HNO_3 concentrations as measured in the stainless steel cell. The lower curve illustrates the behavior of relative transmission through the 25-mm-diam pyrex cell. All of the curves shown in Figs. 11, 12, and 13 can be fit with mathematical functions. Therefore, by making both an x-ray fluorescence analysis measurement and a transmission measurement it is possible to define both the solution concentration and acid molarity. A typical measurement is described in the appendix to this report.

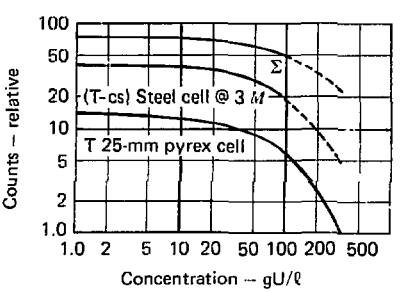

Fig. 13. A log-log plot of the relative number of counts for three parameters vs concentration. The sigma (Σ) is a sum of 5% of the gross incoherent and the transmitted intensity of a 122-keV beam (T-cs) for the stainless steel cell. The bottom curve shows the transmitted intensity through the 25-mm pyrex cell (different beam than that used for the stainless steel cell).

FUTURE RESEARCH AND DEVELOPMENT NEEDS

Before the technique of energy-dispersive x-ray fluorescence analysis can be considered ready for *in-plant installation or an in-plant* test and evaluation, there are a number of experimental parameters that must be further explored or refined. These include mechanical, electronic, computer-based algorithms, and solution requirements. They will be discussed in the order just given, which in effect proceeds from the simplest to the more complex issues confronting the possible use of this technique for monitoring solution concentrations in a reprocessing plant.

Mechanical Requirements

The net count rate obtained from fluorescence of the solutions within the pyrex cells was observed to increase by a factor of 3 going from the 12-mm- to the 25-mm-diam cell, but it increased by only another 20% when the 38-mm cell was used. Thus, for the largest diameter cell, the solution depth is nearly infinitely thick as far as the exciting and fluoresced radiations are concerned. The steel cells used had an effective inside diameter of 1.58 cm compared to 2.2 cm for the 25-mm pyrex cell. The smaller steel cell gave rise to fewer fluoresced K x-rays, but relatively more incoherently scattered events. Its higher atomic number walls [Fe (Z = 26) vs Si (Z = 14)] are closer to the edges of the solid angle accepted by the detector through the heavimet collimator. A larger steel cell would improve the fluoresced signal to Compton-scattered noise level. However, in the event the solution contains a radioactive component (^{239}Pu, ^{240}Pu, ^{241}Pu, or ^{235}U), a larger cell would give rise to an increase in the background noise from gamma-ray radioactivity within the solution volume. The steel cells also have by necessity thicker walls (to simulate a plant pipe), hence an optimum diameter for the steel cell must be defined in terms of whatever detector collimator diameter is selected. In an actual plant situation if the steel pipes cannot be modified, then the detector collimation would be defined by the pipe diameter. For a 1.50-mm-thick stainless steel wall tubing and 12.5-mm-diam detector collimator, it appears that a steel cell 3.5 cm in diameter may give a near-optimum XRFA signal-to-noise level. The optimum diameter should be found. If thicker walls are required in a real plant pipe, then a stronger exciting source strength would be required.

In the event that the XRFA technique is used on either a single-element or dual-element solution in which there is considerable radioactivity (^{235}U or ^{239}Pu, ^{240}Pu and ^{241}Pu), then a shutter mechanism could be designed that would be computer controlled. One position would allow fluorescence, the other would not, hence only the natural radioactivity would be observed. For solutions containing a significant amount of radioactivity, then the count time for fluorescence and radioactivity content would be of equal length. For solutions containing relatively little activity, the radioactivity count time required would be longer to obtain equivalent statistics; however, the correction applied to the fluorescence data would be correspondingly smaller, hence it would need to be less accurately quantified.

A very important consideration for either plant installation or test and evaluation is localization of the dewar-detector, source-exciter-collimator assembly. The detector and analysis system must be calibrated. This will most likely be done using stainless steel cells of very nearly exactly the same physical dimensions as those of the process-stream pipe. Since the dewar-detector assembly would be located in two different places for the calibration measurements vs the actual measurements, some mechanical means must be devised that will positively locate the pipe in exactly the same position as the calibration cells. This localizer should be mechanically coupled to the collimator assembly. Note that the only mechanical requirement prior to carrying out an in-plant test or installation is that the type of stainless steel used in the process-stream pipe, its outside diameter, and its wall thickness be accurately known and defined.

Electronic Requirements

All of the results reported in the section Experimental Procedures and Results were obtained using an analyzer conversion gain of 0.2 keV/channel over 1024 channels. The HPGe detector had a resolution of about 600-eV FWHM for the 122-keV, ^{57}Co gamma ray; hence, there were about three channels at FWHM for a typical 100-keV x ray (uranium or plutonium) and six channels at FWTM. For an in-plant test or installation it would be desirable to spread the spectrum over 4096 channels and include the 200- to 213-keV region. This would allow access to the intensities of the 203.54-keV gamma ray of ^{239}Pu, the 205.31-keV gamma ray from ^{235}U, and the 208.00-keV gamma ray in the decay chain of ^{241}Pu. The conversion gain would be about 0.052 eV/channel, giving typical x-ray FWHM line widths of 10-11 channels at 100 keV for a detector having 550-eV FWHM at 122 keV. This smaller conversion gain would also allow better resolution of close-lying x-ray lines such as uranium Kα1 at 98.439 keV and plutonium Kα2 at 99.536 (peak-to-peak separation of 21 channels at 0.052 eV/channel). Finally, more accu-

rate fitting of the spectral data is possible through the use of sophisticated mathematical x-ray and γ-ray peak shape algorithms. These are discussed in the following subsection.

In the results reported in Experimental Procedures and Results there was evidence of a ±0.3 channel gain drift. This drift could have been in the analyzer, amplifier, or the preamplifier. Although this magnitude of gain drift would be less troublesome if a smaller conversion gain were used (provided it was due solely to the analyzer); nevertheless, the most accurate and reproducible results will be obtained if gain and zero stabilization are employed. At the smaller conversion gain of 0.052 eV/channel, copper would be the better material to line the inner wall of the detector collimator, in addition to the cadmium. This would give rise to a constant source of copper x rays that would serve as an excellent zero stabilization pulse. The Kα1 and Kα2 x rays would appear at 8.04 keV, or about channel 155. If the XRFA system employed a third ^{57}Co source to monitor the solution for density changes (changes in acid molarity), then the transmitted 122.05-keV line would always be present, hence an excellent gain stabilization pulse. Otherwise, one of the fluoresced x rays or one of the natural radioactivity gamma rays could be used.

Computer Software Requirements

The results discussed in this report have been based principally on gross counts within a fixed-channel window. This method works well for single-element solutions at medium to high concentrations without any substantial (<1%) radioactivity content. For single-element solutions with greater than a 10% contribution in the x-ray region from stream activity, or in dual-element solutions where the plutonium contributes radioactivity, the fixed-window method of spectral peak integration is insufficient. In its place, mathematical x-ray and gamma-ray peak shape fitting functions must be used. Such fitting functions can be used to fit very complicated spectra with excellent results.[4] These software codes are written but have not yet been fully implemented on the kinds of spectra obtained in this work. Once they are successfully implemented, many of the equations that currently use total gross counts would be redefined in terms of net counts observed. Also, for weak solutions such a net count calibration would lead to better accuracy. This would eliminate the BK term of Eq. (1).

Solution Requirements

The only dual-element solution made up for evaluation of the XRFA tecnhique contained slightly depleted uranium and aged weapons-grade plutonium. Hence, the isotopics of both elements were not representative of those expected at the output of an LWR fuel reprocessing plant. In addition, americium was present, which would not occur in freshly reprocessed material. To obtain solutions more representative of freshly reprocessed material, chemical separations should be performed on plutonium oxides that have an isotopic composition more nearly like that shown in the two center columns of Table 1. The chemically separated plutonium solution would be concentrated and combined with natural uranium or slightly enriched (~1% ^{235}U) uranium nitrate to obtain the desired concentrations. Then, these solutions would be measured at frequent periods for several months to examine the time-dependent growth of the radioactive decay products. Storage tanks will probably be used at a reprocessing plant, and since solution storage times are not well defined, any measurements made poststorage would have different spectral characteristics than those of the freshly reprocessed prestorage solutions. It is important that these time-dependent results be understood and interpretable, hence the need to simulate these results as closely as possible in the laboratory.

In the event that an in-plant test and evaluation is desired, the detector-excitor system should be more carefully calibrated in the immediate vicinity of the concentration, isotopics, and acid molarities expected in a particular stream. The results presented in the previous section demonstrated that the XRFA technique can be applied over a wide dynamic range of solution concentrations. Clearly, if this technique were installed on one or more streams within a reprocessing plant, these streams would not experience a one-to-two order of magnitude change in concentration. Similarly, the stream's acid molarity would not be expected to span the range 1 to 9 *M*. Instead, concentration, acid stream molarity, and even radioactivity content would vary by small percentages, perhaps even by factors of 2, but not by factors of 10 to 100.

Suppose, for example, that a single-element stream of uranium nitrate was to be monitored and its concentration was 8 ± 2 g U/l, with an acid molarity range of 3 ± 0.3 *M*/l, and enriched in ^{235}U to 50 ± 20%. Then, calibration solutions would be made up at concentrations of 2, 6, 8, 10, 14, and 20 g U/l, all with acid molarities of 3.0 *M*/l and enrichments in ^{235}U of 50%. Additional solutions of concentrations 4, 8, and 12 g U/l would be made up at each of three acid molarities 1, 3, and 5 *M*. Finally, another 8 g U/l solution would be made with a ^{235}U enrichment of 70%; one each 8 g U/l solutions at 30 and 70% enrichment, and a 10 g U/l solution at 30% enrichment. With these in addition to the standard 50% enrichment solutions, the

entire range of variation in the concentration, molarity, and enrichment expected in this stream would be spanned and carefully calibrated. In addition to the fluoresced intensity, the natural radioactivity of each of the different enrichment solutions would be measured; hence it also would be well calibrated.

In the event that dual-element streams are to be monitored, a more careful calibration must be carried out using mathematical algorithms that allow net counts to be determined. Then, the functional forms for the two individual calibration constants, K_U and K_{Pu} would be different than that derived for either of these elements alone in a single-element solution. The exact nature of their functional forms would depend on the concentration ratios. For example, if uranium is present at a concentration seven times that of plutonium, then the fluorescence results for 50 g Pu/l plutonium must be interpreted in terms of a total solution concentration of 400 g/l (350 g U/l + 50 g Pu/l). Thus, not only will the net c/s vs concentration look different, but also the functional form of K_U and K_{Pu} can be expected to differ from those shown in Fig. 7.

ACKNOWLEDGMENTS

We are indebted to many staff members of the Savannah River Laboratory who were helpful throughout all phases of this work. The authors acknowledge the project guidance offered by Drs. R. Swingle and E. Lukosius, the executive direction of Drs. R. Folger and E. Baucom, and Mr. W. Lawless for his administrative assistance. We particularly thank Drs. Kenneth MacMurdo and Major Thompson for their patience in introducing us to the technical subtleties of the various reprocessing cycles and for answering the many technical questions so crucial to a successful research and development program. Also, we acknowledge the Office of Safeguards and Security, DOE, Washington, D.C., whose support through the LLL Safeguards program allowed this interim report to be written.

REFERENCES

1. T. J. Warren, W. E. Prout, M. C. Thompson, M. S. O amoto, and G. S. Nichols, *Technical Data Summary Coprocessing Solvent Extraction Facility*, Savannah River Laboratory, Document DPSTD-AFCT-77 1977).
2. W. D. Ruhter and D. C. Camp, *Nondestructive Assay of Mixed Uranium and Plutonium Oxides Us. ., Gamma Ray Spectrometry*, Lawrence Livermore Laboratory, Livermore, CA, Rept. UCRL-52625 (1978).
3. D. C. Camp, *An Introduction to Energy Dispersive X-ray Fluorescence Analysis*, Lawrence Livermore Laboratory, Livermore, CA, Rept. UCRL-52489 (1978).
4. R. Gunnink, "Computer Techniques for Analysis of Gamma Ray Spectra," in *Proc. Am. Nucl. Soc. Topical Conf. on Computers in Activation Analysis and Gamma-Ray Spectroscopy*, Puerto Rico (1978). Also *Computer Techniques Used in the Analysis of Gamma Ray Spectra*, Lawrence Livermore Laboratory, Livermore, CA, Rept. UCRL-80297 (1978).

RMD

APPENDIX
Concentration Measurement Procedures and Equations

A typical measurement would proceed as follows. First the concentration would be calculated from Eq. (1) (Fig. 7). This yields a solution concentration, C, at the standard operating solution molarity. From this preliminary concentration, C, the amount of coherent scattering can be calculated (Fig. 12). Then the constant Σ is obtained from the sum of a fraction of the observed gross incoherent intensity plus (T-cs). This Σ leads to a new concentration, C′ (Fig. 13). If $C=C' \pm(\sigma_c^2 + \sigma_c^{2\prime})^{1/2}$, then the original concentration calculated is accepted. If the new concentration C′ does not agree with C to within their combined standard deviation, then two values for the solution molarity can be calculated from the (T-cs) and GKαI relationships (Fig. 11). The difference between the standard operating molarity, M, and the two calculated molarities, M_1 and M_2, lead to two small correction factors, C_1 and C_2 (Fig. 12), that are applied to the original concentration. In the next few paragraphs the actual equations obtained for the stainless steel cell will be given, then three examples will be presented to illustrate the use of the equations and the method.

First, an equation is defined for K for the stainless steel tube containing pure uranium solutions with a ^{57}Co "beam" transmission source mounted above it. This equation is

$$\ln K = 5.9716 + 0.5625 \ln R + 0.17986 (\ln R)^2 + 0.01743 (\ln R)^3, \quad \text{(A-1)}$$

where $R = (UGK\alpha I/GI - B)$, and G stands for gross counts. This equation is valid for concentrations $1 < C < 150$ g U/l, which is obtained from the product KR. Also note that because of the additional source scattering material above the cell, Eq. (A-1) is not the same as that shown at the top of Fig. 8. Having calculated a concentration, the 122-keV coherent-scattering contribution from the solution and the stainless steel tube, cs, in counts/1000 s, is given by

$$cs = 3995 + 186 \ln C - 181.4 (\ln C)^2 + 40.6 (\ln C)^3. \quad \text{(A-2)}$$

Then, the sum

$$\Sigma = [0.05\ GI + (T - cs)] \quad \text{(A-3)}$$

defines the constant Σ, where T is the total number of net counts recorded in the 122-keV gamma-ray line. Next, the equation

$$\ln \Sigma = 11.225 - 0.0675 \ln C' + 0.05684 (\ln C')^2 - 0.01362 (\ln C')^3 \quad \text{(A-4)}$$

allows a value of C′ to be calculated using either interpolation or an iterative procedure. It was impossible to find a satisfactory expression for $C' = fn(\Sigma)$. If C does not agree with C′ to within the error $(\sigma_c^2 + \sigma_c^{2\prime})^{1/2}$, then HNO_3 molarity values for the solution must be calculated from the UGKαI and T′ = (T-cs) values. In Fig. 11, both of these were observed to have had a linear relationship with acid molarity; however, their slopes and intercepts will be functions of concentration. Thus, both equations take the form

$$GK\alpha(C') = a_1 + b_1 M_1 \quad \text{(A-5)}$$

and

$$T'(C') = a_2 + b_2 M_2, \quad \text{(A-6)}$$

where

$$a_1 = 11{,}266.6\ C^{0.6705}, \quad \text{(A-7)}$$

$$b_1 = -2.81806\ C^{2.275} (C^{-0.2265})^{\ln C'}, \quad \text{(A-8)}$$

$$a_2 = \frac{39{,}423}{C^{0.001446}} \left[(C^{-0.017519})^{\ln C'} (C^{0.016942})^{(\ln C')^2} (C^{0.004396})^{(\ln C')^3}\right] \quad \text{(A-9)}$$

and

$$b_2 = -48.086\ C^{1.299} (C^{-0.26})^{\ln C'}. \quad \text{(A-10)}$$

Note that C′ should be used throughout in Eqs. (A-7) through (A-10) wherever a C appears. In effect, the coefficients $a_{1,2}$ and $b_{1,2}$ allow the intercepts and slopes of the linear relationship between GKα, T′ and molarity to be calculated. Once M_1 and M_2 are obtained, then $dM_1 = M - M_1$ and $dM_2 = M - M_2$ are obtained. The percentage correction that must be applied to the original concentration, C, is given by

$$\frac{dC}{dM} = -3.24 + 0.5088 \ln C', \quad \text{(A-11)}$$

thus

$$C_1 = (1 + dC_1/100)\ C, \quad \text{(A-12)}$$

$$C_2 = (1 + dC_2/100)\ C. \quad \text{(A-13)}$$

Clearly Eqs. (A-1) through (A-13) are valid only for the stainless steel cell used in this experiment. Once K is defined, the Eqs. (A-1) and (A-11) through (A-13) are independent of source half-life. Equations (A-2) through (A-4) and (A-7) through (A-10) depend on half-life, i.e. the counts obtained must be corrected for time elapsed since defining the functional relationships.

TABLE 4. Examples of actual and simulated concentration determinations.[a]

M	Known (k) or assumed (a) concentration	Measured counts UGKα1	Measured counts GI	$\frac{GK\alpha}{GI}-B$	K_{calc}	Calculated concentration (σ)	0.05 GI	Measured (T-cs)	Σ	C' (σ_i)
3.0	34.92 (k)	120,750	656,500	0.15226	229.0	34.87 (10)	32,825	32,900	65,725	34.64 (23)
3.0	36.75 (a)	124,950	654,400	0.15927	229.8	36.60 (10)	32,720	32,280	65,000	36.80 (23)
?	34.92 (k)	118,600	667,000	0.14615	228.4	33.38 (10)	33,350	32,290	65,640	34.90 (21)

[a]See text for detailed explanation of tabular entries.

Such corrections are easily carried out by the LSI-11 computer.

Consider the three examples shown in Table 4. Note that for the third example the molarity is unknown. The values for K in column 6 are calculated from Eq. (A-1). These K values lead to the calculated concentrations shown in column 7 (errors shown in parentheses). Continuing, we use the parameter Σ derived according to Eq. (A-3) to derive new concentration values, C'. These values are derived from Eq. (A-5) by using either an iterative procedure or interpolation. In the first two cases, the total error $\sigma_t = (\sigma_C{}^2 + \sigma_{C'}{}^2)^{1/2}$ allows overlap between C and C', hence the original concentrations determined from the XRF analysis (column 7) are verified by the transmission measurements. However, for the third case the difference in concentrations (columns 7 and 11) is 1.52 ± 0.23 g U/l. This disagreement suggests a change in the acid molarity. Using the data in columns 3 and 10 (line 3) and the concentration C' (*not* the C from column 7), values for M_1 and M_2 can be calculated from Eqs. (A-5) through (A-10). Equations (A-7) and (A-8) yield $a_1 = 121{,}971$ and $b_1 = -523$. This calculated intercept and slope is to be compared with values of 122,450 and −560 from the least-squares fit to the data shown in Fig. 11. Similarly, Eqs. (A-9) and (A-10) lead to the values $a_2 = 33{,}365$ and $b_2 = -182$, vs 33,350 and about −162 seen in Fig. 11 for th. (T-cs) line. The values of a_1, b_1 and a_2, b_2 yield $M_1 = 6.45$ and $M_2 = 5.95$. Since dM_1 and dM_2 are negative, dC_1 and dC_2 are positive and $C_1 = 1.0494C$ and $C_2 = 1.0422C$. These two small corrections are applied to the original concentration, C = 33.38, shown in column 7. Thus, $C_1 = 35.03$ and $C_2 = 34.79$ for a mean value of C = 34.91 ± 0.12, which is in excellent agreement with the value obtained for C' of 34.90 ± 0.21. The mean solution molarity determined is 6.2. Note that had the solution molarity been less than 3, the concentration calculated in column 7 would have been too large, i.e., C > C', the dM's would have been positive, and the dC's negative. Thus, C would have been reduced.